Mine Water Environ (2016) 35:421–434
DOI 10.1007/s10230-015-0369-x

TECHNICAL ARTICLE

Grain Size Effects on Mine Water Quality and Acid/Neutral Rock Drainage Production in Kinetic Testing Using Recsk Porphyry Skarn Cu–Zn Deposit Rocks

Rodrigo Embile Jr.[1,2,3] · Ingar Walder[1,3] · Ferenc Madai[2] · Ferenc Móricz[2] · Przemyslaw Rzepka[1] · Patrizia Walder[1]

Received: 21 January 2014 / Accepted: 4 October 2015 / Published online: 16 October 2015

Abstract The quality of mine drainage from sulphide-containing waste rock dumps is controlled by several factors. To characterize the effects of grain size on acid/neutral rock drainage production, kinetic tests were performed on samples from the Recsk porphyry skarn Cu–Zn deposit in Hungary, an area known to generate ARD. Five columns were used, each containing specific grain size ranges (1–2, 2–4, 4–8, 8–16, and 16–32 mm). Prior to the kinetic tests, a static test was performed for each grain size range to obtain total and available neutralizing potential (NP) and acid potential (AP). Total NP and AP values were roughly similar for all grain size ranges, while available NP increased as grain size decreased. The neutralization potential ratio for all grain size ranges was <1, which suggests a potentially acid-producing material. The kinetic tests, however, had contrasting results; a grain size of 1–4 mm produced a circumneutral pH, while grain size groups >4 mm produced pHs from 5.1 down to 3.6. Higher alkalinity values in the leach water were linked to the finer grain samples, primarily producing circumneutral pH. Grain size correlated with the sulphate release rate during the stable release period: the sulphate release rate was less at larger grain sizes. In contrast, sulphide oxidation calculated from oxygen consumption was highest for the intermediate grain size range, followed by the coarser and then the finer grains. The leaching of metals established an increasing concentration with increasing acidity without a very clear relationship to grain size. The established concept of increased metal mobility with decreasing pH applies, regardless of grain size.

Keywords Hungary · Column test · Acid Potential · Neutralizing Potential

Introduction

Unlike mine tailings, which are usually uniformly sized, mine waste rocks range from boulder-sized to as fine as clay. This variation has a huge bearing on the leachate quality produced. Smith et al. (1995) made some comparison and characterization of different mine spoils in terms of their grain size distribution. They pointed out that the generation of acidic water within a waste rock pile reflects a complex interaction between hydraulic and chemical processes, among others. The prediction of acid generation in waste rock is usually more difficult than in tailings because of extreme heterogeneity in mineralogy, stacking sequence, and particle size in waste rock dumps (Fergusson and Morin 1991). Although the role of bacteria and Fe(III) in enhancing sulphide oxidation is not discussed in detail in this paper, their effect on the rate of reaction is not discounted.

In this study, we assessed the effects of grain size on the leaching characteristics of materials in kinetic tests. Rock samples from the suspended Recsk "deep-level" −900 m exploration adits in Hungary (Supplemental Fig. 1) were used. (Editor's note: supplemental files accompany the online version of this paper and can be downloaded for free.)

Electronic supplementary material The online version of this article (doi:10.1007/s10230-015-0369-x) contains supplementary material, which is available to authorized users.

✉ Rodrigo Embile Jr.
rodrigofembilejr@gmail.com

[1] Kjeøy Research and Education Ctr, Vestbygd, Norway

[2] Faculty of Earth Sciences and Engineering, University of Miskolc, Miskolc, Hungary

[3] New Mexico Institute of Mining and Technology, Socorro, NM, USA

The sulphide content is normally over 10 wt% of the rock (Földessy and Szebényi 2008) in the Cu–Zn skarn developed between diorite and the limestone units in the area. The natural environmental signatures of the sulphide deposits in the area are concentrated in mineralized and altered zones. The ground and surface waters have an elevated metal content (Rukezo 2003).

Kinetic tests of mine waste are primarily performed to evaluate the likelihood of sulphide-containing waste going acidic or not. Unlike static tests that are usually relatively fast and only give indicative information based on total composition of waste material (CEN/TC 292 2009), kinetic tests take longer but also provide information on reaction rates. In addition, kinetic tests can simulate field conditions of mine waste dumps or tailings to predict drainage water quality. Kinetic testing can be done using humidity cells (ASTM 2007) or columns. A number of published studies have looked into the effects of grain size on kinetic tests. Geidel et al. (1983) and Lapakko et al. (2006) studied the effects of grain size variation in different lithologies. Lapakko et al. (1995) and Morin and Hutt (1994) pointed out the importance of surface area effects on the reactivity of both sulphide and carbonate minerals. Bowell et al. (2006) addressed the influence of particle size on pyrite oxidation and oxygen diffusion. Rosso et al. (1999) looked into the interconnectivity of pore space between different particle sizes and its effects on the diffusion of oxygen. Strömberg and Banwart (1999a) studied the influence of mineralogy and particle size to acidity-consuming processes in mining waste rocks. Jambor et al. (2003) showed that very fine fractions (<0.074 mm) in waste rock can increase its neutralization potential (NP) by as much as four units. Strömberg and Banwart (1999b) also worked on scale-dependent rate factors and pH controls using large column experiments (2 m × 0.8 m). Results from these studies generally indicate that in sulphide-bearing waste rocks, with properly accounted neutralizing minerals, finer-grained material generally tends to produce a more acidic pH. However, as discussed below, and backed by previous studies, this may not always be the case.

Methodology

Material Characterization Prior to Kinetic Testing

Bulk rock samples were obtained from an old rock dump coming from −900 m level of the Recsk porphyry skarn Cu–Zn deposit. The rocks collected were fairly large (15 cm × 15 cm × 15 cm) and were crushed to obtain the fresh core for further size reduction. Rock surfaces were cleaned and oxidized surfaces, where present, were removed. The samples were then thoroughly blended before final crushing and sieved into 3 kg of five different grain size ranges, namely 1–2, 2–4, 4–8, 8–16, and 16–32 mm.

Material characterization was completed before and after kinetic testing at the Institute of Mineralogy and Geology, University of Miskolc. The methods used were X-ray powder diffraction (XRD) for mineral composition, X-ray fluorescence (XRF) for bulk chemical composition, liberation analysis under stereo microscopy to estimate the available mineral surfaces, and static tests for acid potential (AP) and NP determination. To obtain information on the mineralogical composition for each grain size range, a combination of XRD and scanning electron microscopy (SEM) coupled with energy dispersive spectrometry (SEM–EDS) was used. SEM and microprobe analysis was performed using a JEOL JXA 8600 Superprobe. Both backscattered (BSE) and secondary electrons (SE) methods were used to image the grains. Petrography analysis was also performed on both fresh and leached samples. Component surface areas were assessed to estimate the percent pyrite and other minerals for each grain size. For the larger fractions (16–32 to 4–8 mm), the phase ratio was estimated based on the total surface, but for the smaller fractions, only the visible surface was used. For the XRD analysis, a representative sample from each grain size group was ground to less than approximately 5 μm in size by hand grinding in an agate mortar and pestle. The analysis was carried out using a Bruker D8 Advance XRD with Rietveld refinement with the following settings: Cu-Kα source, 40 kV and 40 mA; Bragg–Brentano geometry; $2\theta = 2°$–$70°$ domain, with goniometer speed of 0.04° (2θ) in 2 s. To complement mineralogical identification, bulk quantitative chemical analysis was done on every grain size by a Rigaku type (200 W Pd X-ray source, 50 kV and 4.0 mA) wave length X-ray fluorescence (WDXRF) machine.

Static Testing

Static testing was conducted based on the European Committee for Standardization (CEN) standard 15875 (CEN/TC 292 2009) to determine the AP and NP of the samples. Total NP (samples milled to <0.125 mm) was obtained for all the grain size groups. Available NP (samples are whole grains), which is based on the modified Sobek method, was undertaken for the finer and intermediate grains sizes (8 mm and less). Available NP was not undertaken for the coarser grain sizes due to strict compliance with the EU method, which suggests that 2 g of sample should be used, since 2 g of sample would constitute one or two grains of these coarser grain groups, making the analysis potentially non-representative (subject to bias of using either a highly pyritic or carbonate-rich grain). The neutralization potential ratio (NPR), which is NP/AP, was then calculated.

Kinetic Testing

Five clear 24 cm tall acrylglas-PLEXIGLAS® columns with an internal diameter of 20 cm, and with a 5–10 um pore cellulose membrane filter fitted at the bottom were used for the set up (Supplemental Fig. 2). Humidified air was continuously supplied and maintained by an air pump connected to the bottom of the column by a propylene tube with no inline filter. A 1.0 cm space from the cover to the rim of the column was left open to allow air outflow. The laboratory temperature was maintained at about 20 °C. To flush out secondary minerals and other oxidation products, the columns were rinsed weekly with 1000 mL distilled water for 85 weeks.

The weekly rinsing was done in two intervals of 500 mL, with 1 h in between, using a bottle with a perforated cap. For each interval, the rinsing was divided into three portions with about 5 min intervals in between. This was done to rinse off possible secondary minerals and precipitates that may have formed during the week. To collect the leachates, the tubes connecting each column to the air pump were temporarily disconnected. Leachates were collected in a beaker after 3–4 h of settling time to optimize collection. Before resuming the humidified flow after the rinsing, the tubes connecting to the columns were carefully inspected to remove possible trapped air bubbles and leachate residues that might have blocked air flow.

Oxygen consumption was measured during weeks 18, 49, and 75, which roughly corresponded to the early, middle, and later stages of the experiment. Measurement was carried out using Quantek Model 902D Dual Trak oxygen/carbon dioxide analyser. The columns were sealed for 9 days during the first sampling and subsequently adjusted to 5 days to coincide with the weekly rinsing cycle. Adjustment for the number of readings obtained was also adjusted from five, three and finally to four measurements for weeks 18, 49, and 75, respectively. The equipment has a needle-type gas collector, which is pierced through the sealant on top while the reading is undertaken.

Leachate Analysis

The collected leachates were weighed and analysed for pH, pe, TDS (total dissolved solids), conductivity, salinity, and alkalinity. The pH and pe were measured using OAKTON pH 2100 and 110 portable meters respectively. TDS, conductivity, salinity, and temperature were measured using a HACH sensION 5 instrument. Alkalinity was measured using Metrohm's Tiamo with 0.01 M HCl as the titrating acid. After completing all the routine chemical tests, the leachates were filtered using a Millipore filtration assembly, with a 0.2 μm diameter cellulose-acetate membrane filter. Two sets of 200 mL samples were collected, one of which was acidified with 50 μL of HCl to inhibit precipitation. The samples were then refrigerated at a controlled temperature of 5 °C. Ion chromatography (IC) was used to measure Ca^{2+} and SO_4^{2-}, using Metrohm 861 Advanced Compact IC equipment with dual ion capability and two columns. Deionized water generated by an ELGA OPTION-Q7 water purifier was used for all sample preparation and solution making. Dilution with deionized water was used to achieve values that were within the range of the standards used. Calibration was done prior to analysis of each group. Consequently, calibrated standards and blanks were inserted randomly during the sample batch analysis.

Atomic absorption spectrometry was carried out using an Analytik Jena® Contra 700 with an acetylene/air flame to obtain Fe, Cu, Pb, Zn, and Mn concentrations in the leachates. Zn was also analysed after a 1/10 dilution due to its relatively high concentration in all the leachates. The equipment was first optimized to achieve optimal absorbance and sensitivity.

PHREEQC (Parkhurst and Appelo 2012) and the PHREEQC database were used to simulate leachate compositions and to obtain Fe^{3+}, Ca^{2+}, SO_4^{2-}, and Cu^{2+} activities. HSC Chemistry was used to create the Eh–pH diagrams using the data obtained from PHREEQC simulations.

Results

Mineralogy

Qualitative XRD analysis performed for each grain size showed fairly uniform amounts of the major rock forming minerals (Table 1). This can be seen in the fairly matched XRD peaks for each grain size group (Supplemental Fig. 3). The diffractograms show that the mineralogical composition was almost the same for each size fraction. In

Table 1 Sample mineralogy from XRD analysis

	Grain size (mm)				
	1–2	2–4	4–8	8–16	16–32
Pyrite	35.4	34.2	33.5	30.0	39.1
Quartz	44.7	42.1	42.3	42.4	39.2
Calcite	7.5	10.2	8.3	5.2	1.9
Dolomite	2.7	0.9	2.7	6.7	9.7
Ankerite	4.1	4.2	7.0	8.0	5.9
Chalcopyrite	1.6	1.9	1.9	1.2	1.0
Sphalerite	3.3	5.5	3.9	6.3	2.2
Titanomagnetite	0.7	0.6	0.3	0.1	0.3
Hercynite	0.1	0.5	0.1	0.1	0.7

the finer fractions, there was more calcite and less dolomite + ankerite, while the reverse was true for the coarser fractions. The intermediate grain size, 4–8 mm had approximately equal concentrations of the two carbonate mineral groups. These variations are possibly caused by differences in the compressibility strength of each mineral during crushing, which resulted in differences in mineral liberation.

XRF analysis showed that the mineral assemblage of major oxides and trace metals were fairly uniform for each grain size (Table 2). The higher standard deviations (SD) for SiO_2, S, and Pb can be attributed to the fact that heterogeneity in the amount of these minerals per grain is very likely, and cannot be fully controlled. SiO_2 covered about one-third of the mass of the analysed material, while Pb was present at very small concentrations. Precision becomes more difficult for relatively high and low concentrations. The XRD and XRF results indicate that there were minor differences in the composition of different size fractions. Nevertheless, it is important to mention that qualitative XRD cannot consider the amorphous phases, so the result is normalized to the amount of the crystalline phases. This causes the small differences in the values reported for the mineralogy and composition using XRD and XRF.

Supplemental Table 1 shows the areal fractions of different mineral phase surfaces for each grain size, which were obtained by area estimation under stereo microscope. Fe oxides/hydroxides represent mainly altered surfaces of pyrite grains. Overestimation of mineral composition is evident; sphalerite for example, is more than twice the average for the 2–4 mm size range. Estimation for smaller grain size samples is therefore less precise.

SEM analysis showed that pyrite generally appears as cubic particles with smooth surfaces. Secondary mineral formation was evident on most grains inspected (Fig. 1). The bulk of these secondary minerals were Fe oxides/hydroxides (e.g. ferrihydrite and goethite), with others being mainly metal sulphates (e.g. $FeSO_4$), metal carbonates (e.g. $ZnCO_3$), metal oxides (CuO), and gypsum. Jarosite was also noted on grains coarser than 4 mm.

Static Test

Static testing showed close ranges for both AP and NP for all of the grain sizes (Table 3). The sulphur content from each grain size (Table 2) had higher non-uniformity (SD of 1.21) than most major elements reported. It is important to note that AP is a record of the total sulphur in the sample, but that variations in concentrations can also be due to sphalerite.

Comparing the four tables shows that the 16–32 mm fraction had relatively higher pyrite and lower calcite than the finer grained fractions. This could be the result of crushing, wherein harder minerals (e.g. quartz and pyrite) are difficult to disaggregate, while less cohesive minerals (e.g. calcite) tend to break apart easily. This is also reflected in coarser grains having less total NP.

Leachate Chemistry

Results of the weekly analytical tests were plotted as time series curves (Fig. 2). For brevity, 1–2 and 2–4 mm will be referred as finer grains, 8–16 and 16–32 mm as coarser grains, and 4–8 mm as the intermediate grain size. Finer grained samples produced circumneutral pH throughout the test, while coarser materials, including the intermediate grain size, produced acidic pH starting at 6.0, 5.2, and 5.0, dropping to 4.2, 3.6, and 4.0 for the 4–8, 8–16, and 16–32 mm fractions, respectively (Fig. 2a). Finer grained

Table 2 Sample mineralogy from XRF analysis

Grain size	SiO_2 (%)	Al_2O_3 (%)	MgO (%)	CaO (%)	Na_2O (%)	K_2O (%)	Fe_2O_3 (%)
1–2	34.4	2.42	4.13	8.34	0.10	0.07	29.41
2–4	33.3	2.36	4.17	8.21	0.12	0.08	29.50
4–8	36.9	2.10	2.93	8.08	0.11	0.14	27.02
8–16	33.1	2.89	4.51	7.86	0.10	0.28	28.32
16–32	34.6	3.37	3.94	5.48	0.11	0.19	30.13
SD	1.35	0.45	0.54	1.07	0.01	0.08	1.10

Grain size	MnO (%)	TiO_2 (%)	P_2O_5 (%)	S (%)	Cu (%)	Zn (%)	Pb (ppm)
1–2	0.347	0.09	0.06	24.17	0.38	1.04	31
2–4	0.389	0.09	0.06	22.74	0.36	1.24	25
4–8	0.302	0.07	0.06	24.61	0.38	1.26	28
8–16	0.320	0.08	0.06	23.51	0.14	1.01	36
16–32	0.123	0.12	0.07	26.33	0.36	0.71	26
SD	0.09	0.02	0.00	1.21	0.09	0.20	3.97

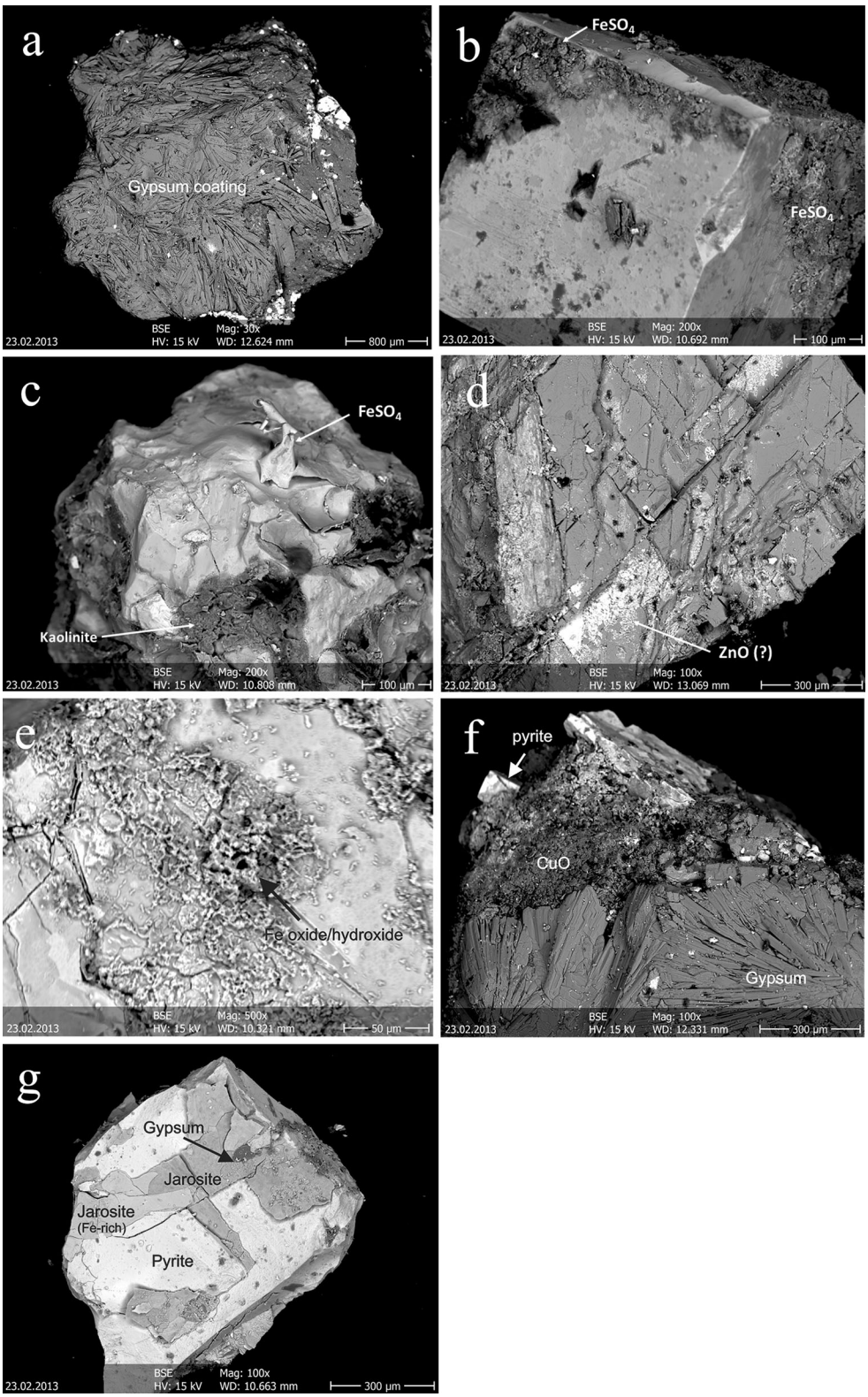

Fig. 1 Selected grain, liberated pyrite and calcite with observed secondary mineral formation on their surfaces. Pyrite grains are usually cubic, with average thickness of about 500 µm. **a** Grain coated with gypsum, **b** pyrite with $FeSO_4$ development, **c** pyrite-rich grain with $FeSO_4$ film and kaolinite clay (*dark coating*), **d** grain of calcite with suspected ZnO film (*bright spots*), **e** pyrite grain coated with Fe oxide/hydroxide, **f** a grain with gypsum and CuO coating, **g** a pyrite grain with jarosite development on its surface

Table 3 Static test results

Static test parameter	Grain size (mm)					SD
	1–2	2–4	4–8	8–16	16–32	
Acid potential (mol H^+/kg)	15.11	14.21	15.38	14.69	16.46	0.76
Neutralizing potential, NP_T (mol H^+/kg) – total	2.69	2.55	2.41	2.49	2.31	0.13
Available neutralizing potential (mol H^+/kg)	2.37	1.56	1.37	–	–	0.43
Neutralization potential ratio (NPR = NP_T/AP)	0.18	0.18	0.16	0.17	0.14	0.01

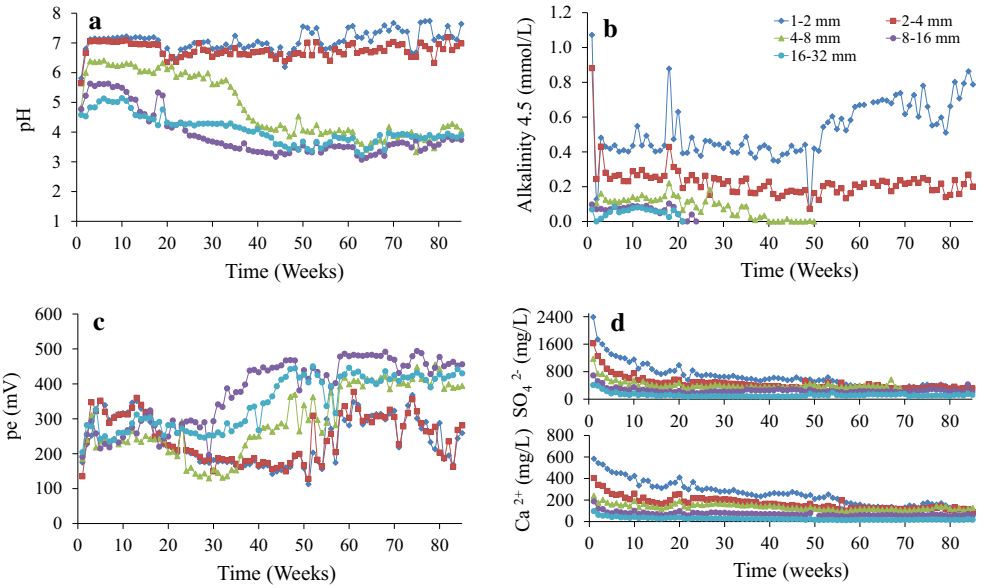

Fig. 2 Kinetic test chemical parameters: **a** pH, **b** alkalinity, **c** pe, **d** SO_4^{2-} and Ca^+

samples achieved stable alkalinity throughout the experiment in the range of 0.35–0.50 and 0.15–0.3 mmol/L for 1–2 and 2–4 mm respectively. By week 40, 1–2 mm showed an increasing trend. Coarser grains, however, showed very low alkalinity values (0.04–0.10 mmol/L), which eventually dropped to zero around week 20 for 8–16 and 16–32 mm and week 35 for 4–8 mm (Fig. 2b). Oxidation–reduction potential (pe) showed a distinct contrast between finer and coarser grains. Finer grains generally followed the same decreasing trend, while the pe for coarser grains increased continuously after week 15 (Fig. 2c). The SO_4^{2-} and Ca^+ plot (Fig. 2d) shows decreasing concentrations over time, where finer grain sizes released more species than the coarser sizes. This trend also supports increased dissolution of minerals with greater surface areas.

Metal Concentrations

Copper evolution over time showed a clear demarkation between different grain sizes (Fig. 3). The finer grains had the lowest concentrations (0.01–0.03 mg/L), while the coarser grains had values from 0.20 to 1.30 mg/L. The intermediate grain size showed a more pronounced increasing trend, starting from 0.07 to 1.1 mg/L. The intermediate grain size also reported the highest initial Cu concentration at 10.30 mg/L. Iron was generally below the detection limit (0.001 mg/L) for the 1–2 and 2–4 mm columns. Average Fe concentrations were more elevated for the 4–8 mm, followed by the 8–16 mm, and then finally the 16–32 mm, with 1.22, 1.16, and 0.46 mg/L, respectively (Fig. 3). The behaviour of Zn over time was generally stable for the 1–2, 2–4, and 16–32 mm size ranges, while the 4–8 and the 8–16 mm had the highest Zn concentration towards the end of the test. The highest recorded concentration was 30 mg/L for the intermediate grain size. Lead was generally below detection limits (0.001 mg/L) for all the grain sizes (Fig. 3). An unusual increase in Pb was observed towards the end of the test for the 2–4 mm. The sudden peaks at week 50 for most of the plots is believed to be related to the oxygen availability measurement during week 49. The Mn plots show a relatively stable and uniform trend for all grain sizes until around week 35, when a decreasing trend was observed (Fig. 3). The finest grain size, 1–2 mm, decreased at a faster rate than the rest.

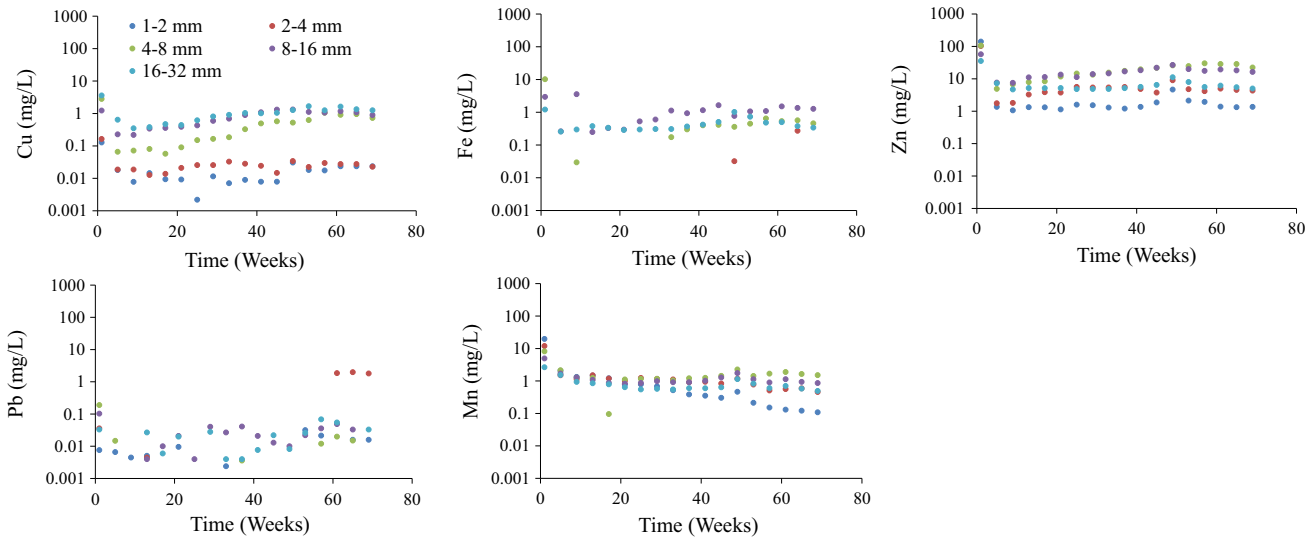

Fig. 3 Metal concentrations over time based on analysis performed for every fourth sample; data are only presented until week 69

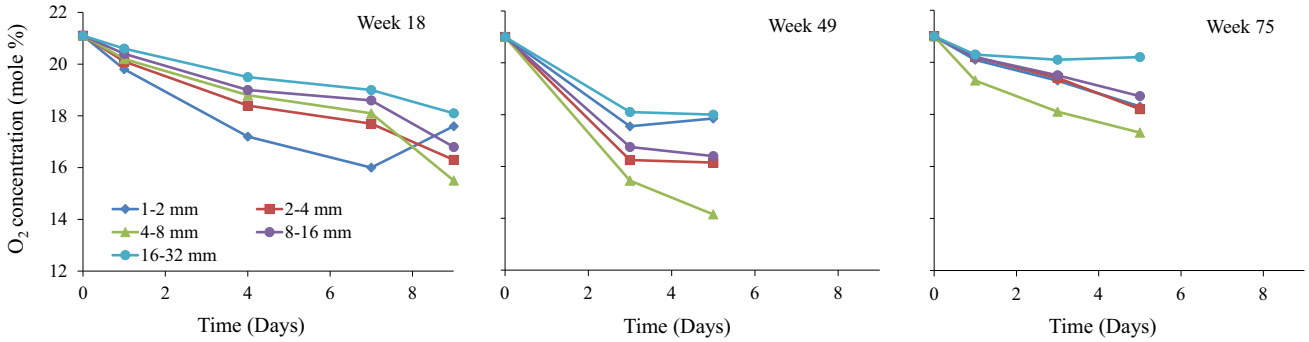

Fig. 4 Oxygen availability plots

Oxygen Availability

The three readings for oxygen availability registered different trends (Fig. 4). For week 18, finer grains generally achieved low final O_2 concentration at 15.3–17.6 mol% O_2. The intermmediate grain size, however, overtook the finer grains towards the 7th day. For week 49, the 4–8 mm registered the lowest final concentration at 14.2 mol% O_2. For week 75, the intermediate grain size still had the lowest O_2 concentration throughout the test, followed by the finer grains and then finally the coarser grains. The observed flattening or increasing trend towards the end of measurement on some columns is indicative of a leak. Data from this period was not used for the interpretation.

Discussion

The material used for this experiment contained significant carbonate mineralisation (calcite + dolomite + ankerite) as well as amphiboles and plagioclase feldspars, which could potentially neutralize the system for a long time, with calcite being the main neutralization driver. The static test results suggest that all of the grain sizes ranges were roughly similar for both total NP and AP and that all showed an NPR <1, suggesting that the neutralizing capacity of the material was not enough to neutralize the acid that will be produced over the long run. Available NP, on the other hand, increased as grain size decreased. This can have a significant effect on the resultant pH. However, it is important to note that neutralization capacity is controlled by many factors in addition to grain size, such as the hydraulic mechanisms between grains, oxygen availability, weathering rate of silicate minerals, formation of secondary minerals, and even experiment duration.

The reduced grain size offers greater reactive surface area for both sulphide oxidation and neutralization. It can be inferred that a balance between these two reactions is more evident for the finer grains, as indicated by circumneutral leachate pH throughout the test period (Fig. 2a). This can also be linked to the relatively higher available NP of the finer grains compared to the intermediate grain

size and possibly to the rest of the coarser grain size ranges. The drop in pe of the finer grains from week 13 also suggests a more reducing environment, which may result in less acid production (Fig. 2c). The alkalinity plot though clearly showed that the acid neutralizing capacity of the 2–4 mm sized sample was maintained throughout the experiment, while an increasing trend was observed from week 50 for the 1–2 mm batch (Fig. 2b).

Coarser grained samples have less surface area available for sulphide oxidation and neutralization. The leachates had a stable, acidic pH in the beginning, between 5.0 and 6.0, until week 10, suggesting a balance between the oxidation of sulphides and neutralization by carbonate minerals (Fig. 2a). This was supported by a stable alkalinity of 0.07 mmol/L. The gradual decrease in pH from week 10 suggests an increasing oxidation rate and, in response, a decreasing acid-neutralizing capacity. This was supported by an increased pe (Fig. 2c). For the 16–32 mm material, there was a short-lived lowering of pH, which became more stable until around week 40, when a second episode of decreasing neutralization capacity occurred. For the 8–16 mm material, a continuous steady decline was observed until about week 45, when the pH stabilized between 3.5 and 4.0. This was supported by an increasing redox potential. In terms of alkalinity, the coarser grained material had no alkalinity from week 20 (Fig. 2b). At this point, almost all of the neutralizing minerals must have been unavailable for reaction, most likely due to the coating effect of secondary minerals, such as gypsum (Fig. 1a). The acidic pH observed for these coarser grains may also be linked to less available NP, relative to the finer-grained material.

Grain size 4–8 mm showed the most distinct trend in pH, pe, and alkalinity. There was a steady decline in pH, from about 6.5 to 5.9 until week 35, and then a decrease to 4.0 during week 40. The pH finally stabilized at the end of the test, possibly reflecting a shift into a more oxidation-dominant reaction (Fig. 2a). This was also clearly supported by the alkalinity, which dropped to zero during week 35 (Fig. 2b). This time period had an increased pe, suggesting an environment that had become more oxidizing or had a more effective oxygen supply. Also, due to the lower pH, Fe has more control over the pe. This is similar to what was observed in the coarser grained material. Dissolution of secondary sulphate minerals, such as jarosite (Fig. 1g), may have also contributed significantly to acid generation for this grain size group.

The marked differences in the above parameters (pH and alkalinity) can be explained by the grain size distribution within the columns and how the grains were connected or separated, such that reactions were able to effectively proceed. Jambor et al. (2003) suggested that very fine particles (<0.074 mm), such as may exist on the surfaces of the grains after size reduction, can enhance NP. It is inferred that these increases occurred, since the surface area of the material increased. It is also likely that most of these particles remained trapped in the finer intergranular pore spaces of the 1–2 and 2–4 mm during rinsing, while for the coarser grains, they ended up at the bottom of the columns after rinsing, thereby limiting their potential contribution. In terms of grain interconnectivity, Lapakko et al. (1998) suggested that physical factors associated with the finer size fractions may enhance the interaction of acidic and alkaline components, since reduction of particle size decreases the distance between sulphide and carbonate mineral grains. They also pointed out that this provides intimate contact, while the retained moisture can also provide a transport medium for the produced acid to reach the neutralizing minerals. Strömberg and Banwart (1999a) observed that calcite within particles >5–10 mm reacts too slowly to neutralize the acid produced from sulphides. The Ca concentration level (20 mg/L) of the coarser grains towards the end (Fig. 2d) also suggests that H^+ was still being consumed by the carbonates, maintaining a pH of 3.5–4.

Hydraulic Factors and Oxygen Availability

Oxygen can move within a waste rock pile by a number of different mechanisms, including diffusion in the gas phase, air convection or advection, and as a solute (dissolved) in the water phase (Walder and Stormont 2004) and is likely a combination of these, with potential seasonal variations. Air movement in the columns can represent a smaller section in a waste dump, with a high flow of convective air in coarser grained areas and diffusion into particles and finer-grained areas. The oxygen consumption plot depicts this effect (Fig. 5). Bowell et al. (2006) related the influence of particle size on pyrite oxidation and oxygen diffusion using data from six kinetic tests with grain sizes ranging from <100 μm to about 8 mm. In their results, diffusion limited the oxidation rate of finer grains due to high water retention, while it was mostly surface area that controlled the oxidation rate for coarser grains. The very fine grains that were efficiently trapped in the pores of the 1–2 and 2–4 mm may have also contributed to the increased neutralization capacity. For the coarser grains, although the surface area of the material was relatively less than the finer grains, oxygen availability was not as limited. Rosso et al. (1999) proposed that under intermediate conditions, the pores in the solid media (especially large pores) are partially gas-filled and create interconnected channels through which oxygen can diffuse more rapidly. At the air–water interface, O_2 is dissolved in the H_2O, creating more aggressive oxidation of exposed sulphide

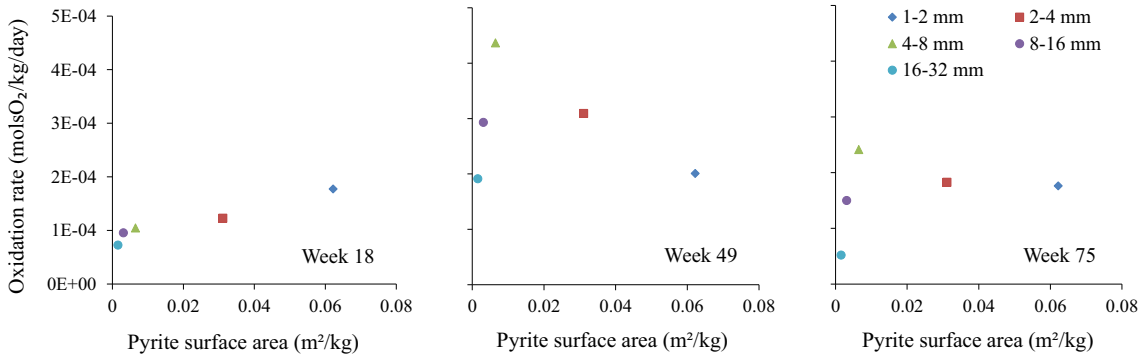

Fig. 5 Oxidation rate versus surface area

Table 4 Main parameters and sulphide oxidation rates for week 75

Grain size (mm)	Initial pH	Final pH	Surface area (m^2/kg)	Sulphate release rate *LR* (mg/kg/week)	Sulphide oxidation rate by O_2 consumed, R_{FeS_2} (mmol O_2/kg/day)
1–2	7.12	7.64	1.24E−02	97.97	0.18
2–4	7.05	6.98	6.22E−03	103.72	0.18
4–8	6.38	4.04	3.25E−03	118.21	0.24
8–16	5.63	3.74	1.56E−03	67.91	0.15
16–32	5.13	3.89	7.78E−04	43.91	0.05

surfaces. The results of Bowell et al. (2006) and Rosso et al. (1999) supports this, as seen in the week 49 and 75 plots of oxidation rate against surface area (Fig. 5), where the intermediate grain sized material had the highest oxidation rate. This was also supported by the sulphate release rate of the finer grains being almost twice that of the coarser grains (Table 4).

Sulphide Oxidation Rate

According to Lapakko et al. (1998), the surface area of a particle is a function of the amount of mineral present, its grain size, the extent to which it is liberated from the rock matrix, and surface morphology [e.g. surface roughness (SR)]. With only a slight dependence on pH (Lapakko et al. 1998), the rate of oxidation is linked to the exposed surface area of sulphide minerals and consequently to the available oxygen.

Pyrite concentration was 22 times that of chalcopyrite (Table 1), which also reacts much slower than pyrite (Acero et al. 2009; Rimstidt et al. 1994). It is therefore reasonable to assume that pyrite is the main sulphide being oxidized in the system. In an environment where oxygen is assumed to be the main oxidizing agent, the rate of this consumption can be expressed in an equation where iron is oxidized from ferrous to ferric and sulphide to sulphate (CEN/TR 16363 2012) (Eq. 1).

$$R_{FeS_2} = \frac{\left(p_{I(O_2)} - p_{F(O_2)}\right)}{t \times 3.75 \times M_{py}} \quad (1)$$

where R_{FeS_2} is the rate (mol O_2/kg/day), $P_{I_{(O_2)}}$ is the number of moles of O_2 initially in the confined space, $P_{F_{(O_2)}}$ is the number of moles of O_2 at the end of the measuring period in the confined space; t is the time (days); M_{py} is the mass of the pyrite in the sample at the start of oxygen depletion measurement (kg); and 3.75 is the ratio of moles of O_2 per moles of pyrite. Sulphide oxidation rates were derived from the three oxygen availability data, corresponding to the early, middle, and late stages of the experiment. This equation, however, does not consider the contribution of Fe^{3+} as a significant oxidizing agent to the remaining pyrite in the system at pH <4.5 (Nordstrom 1982).

To establish the possible relationship between surface area and oxidation rate, a plot of these two variables was created (Fig. 8). In calculating the surface area in each column, the formula presented by Lapakko and Antonson (2006) was used (Eq. 2).

$$A_{py,i} = \left(\frac{\%S^{2-}}{100}\right)\left(\frac{55.85 + 64.12}{64.12}\right)\left(\frac{6}{\rho d_{gm,i}}\right)\left(\frac{M_i L_i (SR)}{100}\right) \quad (2)$$

where $A_{py,i}$ is the pyrite area in a particle size fraction (m^2); $\%S^{2-}$ is the percentage sulphide (S^{2-}) of sample in the size

fraction, i; ρ is the pyrite density equal to 5.02×10^6 g m^{-3}; d_{gmi} is the geometric mean diameter of particle size fraction i (m); M is the mass of rock in particle size fraction i (g); L_i is the percent pyrite exposure in particle size fraction i; and SR is the surface roughness (SR) factor for pyrite, estimated as 2.6 (Parks 1990) for pyrite with smooth surfaces. Pyrite liberation (L_i) is the degree to which pyrite is separated from the rock matrix, which generally increases during grain size reduction. This can be attributed to the fact that the smaller pyrite grains are more easily removed in the finer-grained material. By counting loose grains, we observed that the finer grains were roughly 5 % pyrite, while the coarser grains, including the 4–8 mm range, was about 2 %. The SR of 2.6 that we used in our calculation is at the lower end of the SR range reported for pyrite (Lapakko and Antonson 2006).

The plot of the pyrite surface area against oxidation rate shows a typical linear trend, where oxidation rate increases with decreasing grain size (Fig. 5) for week 18. This supports the concept that greater surface area promotes higher oxidation rates. However, a significant rate change can be seen starting at week 49. The intermediate grain size 4–8 mm registered the highest oxidation rate, at 0.43 mmol O_2/kg/day, followed by the 2–4, 8–16, and finally the 1–2 mm range. The rate for 16–32 mm was not considered due to the leakage observed on the fifth day. The oxidation rate for week 75 represents the actual rate for each grain size, since this was part of the period when stable sulphate release was observed in each column. The intermediate grain size still had the highest oxidation rate at 0.24 mmol O_2/kg/day, followed by the 1–2 and 2–4 mm grain size, which had almost the same rate at 0.18 mmol O_2/kg/day (Fig. 5; Table 4). This, however, only explains one aspect of these results. The reason why the finer grains, with the greatest surface area, achieved circumneutral pH is explained below.

Sulphate Release Rate

Sulphate release or leaching rate was calculated using the equation by Price (2009) (Eq. 3). To get the general leaching rate, the average concentration of SO_4^{2-} and volume of the leachate during stable release were used. This varies for each grain size (Table 4).

$$LR = \frac{C_r \times V_r}{M_s \times t_r} \quad (3)$$

where LR is the leaching rate (mg/kg/week); C_r is the constituent concentration in the rinse (mg/L); V_r is the volume of the rinse (L); M_s is the mass of the sample (kg); and t_r is the time between each rinse interval (week). This assumes that all SO_4^{2-} released is from pyrite oxidation and that all of the SO_4^{2-} was removed by rinsing.

The onset and duration of stable sulphate release rate varies for each grain size group. The relationship of sulphate release rate to pH has been well-established by previous studies. Morin et al. (1995), looking at the statistics of kinetic test results, pointed out that samples generating the lowest acidic pH had the highest average rate of sulphate release. This contrasts somewhat with the results of this experiment, where the highest sulphate release corresponded to the finer grains, but with a circumneutral pH (Fig. 6). This suggests that factors other than surface area may play a significant role. Two such possible factors are water saturation and oxygen availability in the system. The high sulphate release rate in the finer grains may be indicative of higher oxygen availability in both the gas and dissolved phases. The finer grains can be saturated with water during and right after rinsing. This period of increased water saturation until evaporation and subsequent rinsing can limit sulfide oxidation and acid production. A correlation of sulphate release and sulphide oxidation rates between each grain size can also be observed (Fig. 6). These results partly contradict the results of previous studies (e.g. Anderson et al. 1999), in which they observed an increasing oxygen consumption rate as particle size decreased. The effect of finer grains can be more significant in increasing the reactive surface area of a system. However, as deviations from ideal trends do exist, possible explanations, as described by Anderson et al. (1999), could be cleavage fractures, SR, and other factors such as the irregular distribution of sulphide minerals on the surface of the waste rock particles.

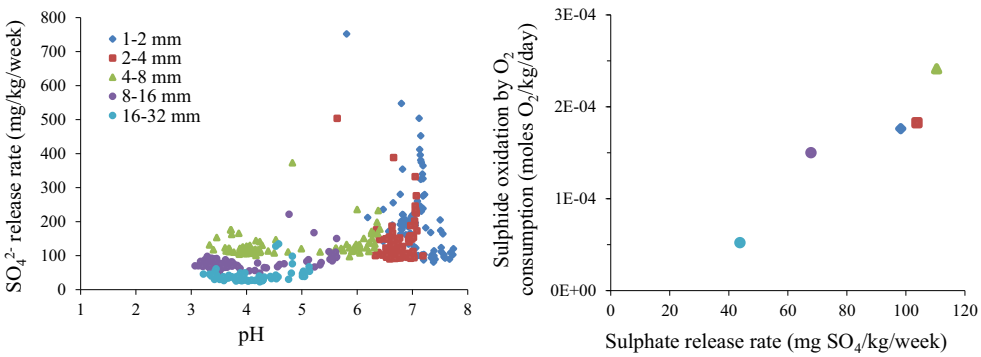

Fig. 6 (*Left*) sulphate release rate versus pH shows that high sulphate release rate does not always result in an acidic pH. (*Right*) sulphide oxidation rate versus sulphate release rate shows a good correlation of these two parameters. Note that the 4–8 mm fraction had the highest oxidation rate and sulphate release, followed by the finer and coarser grains

Secondary Mineral Formation

Secondary minerals on the sulphide and carbonate mineral surfaces can reduce the available surface area for oxidation and neutralization, respectively. The reaction between sulphate from sulphide oxidation and Ca from carbonate dissolution may result in saturation and precipitation of gypsum (Price 2009). Because of its wide range of solubility, gypsum removal was a major concern as this can dramatically affect sulphide oxidation rate calculations. When sulphide oxidation is high and gypsum precipitates, the column rinse water incorrectly provides a lower calculated rate than the actual reaction rate. At some point, when the sulphide oxidation falls below some critical value, the accumulated gypsum begins dissolving, so that the rinse water incorrectly provides a higher calculated rate than the actual rate (Morin et al. 1995). The Cu, Zn, and Pb concentrations reflect the oxidation of chalcopyrite, sphalerite, and galena while Mn may be coming from sphalerite. Molnár et al. (2008) reported that sphalerite can contain elevated Mn (2–4 %). Water-soluble oxidation products reporting to the leachate can indicate if secondary minerals are being stored within the grains or are being flushed out effectively. In this experiment, the finer grains size stored oxidation products quite efficiently, but during rinsing, most of these were washed out, thereby giving rise to higher concentrations of these ions.

By plotting the log of the Fe^{3+} and Cu^{2+} activities, it was found that tenorite (CuO) controls Cu concentrations in the finer grains, while goethite [FeO(OH)] and ferrihydrite [$Fe(OH)_3$] control Fe^{3+} concentrations for the coarser and finer grains, respectively (Fig. 7). Other secondary iron minerals may also possibly be controlling total Fe concentration.

Neutralizing Mechanisms Other than Calcite

Mine waste drainage will not acidify as long as the rate of acid neutralization equals or exceeds the rate of acid production. This, to a large degree, depends on the relative surface areas of iron sulphide and calcium carbonate (Lapakko et al. 1998) and silicate minerals (Lapakko et al. 2006) available for reaction. Weathering of feldspars, for example, produce clay minerals that can slow down the oxidation rate in two ways. First, feldspar dissolution consumes acid. Second, clay mineral development can impede oxygen and water transport, thus limiting further sulphide oxidation. In addition, according to Lapakko (1988), these minerals (i.e. anorthite and forsterite) dissolve more rapidly as pH decreases; however, the rate of acid production must be relatively slow for this dissolution to maintain circumneutral pH. The presence of amphiboles and plagioclase feldspars and their weathering to clay minerals such as kaolinite may have slowed down further oxidation of the system in the finer-grained runs, such that the acid production was generally stable throughout the experiment.

Role of Bacteria

Although the presence of bacterially enhanced sulphide oxidation is not discussed on this paper, the contribution of bacterial activity, such as that of *Acidithiobacillus ferrooxidans*, may have significantly contributed to the higher oxygen consumption rate in the coarser grains, most especially for the 4–8 mm. As pH further decreases, bacterial oxidation of Fe^{2+} becomes the rate limiting step in the oxidation of pyrite by Fe^{3+} (Hallberg 2010; Schippers et al. 2010; Singer and Stumm 1970).

Phase Stability Diagrams

To better understand the mineral formation and stability of some ionic and mineral species in the leachates, Eh–pH plots were generated using HSC Chemistry® software by Outotec. It must be noted that the stability ranges of the mineral species (i.e. gypsum and ferrihydrite) is only that of the leachates and does not reflect actual mineral formation and stability in the grains inside the columns.

Ca–S–H_2O System

The phase diagram of Ca and S indicates that the stability of gypsum is best captured in the finer grains (Fig. 8). The

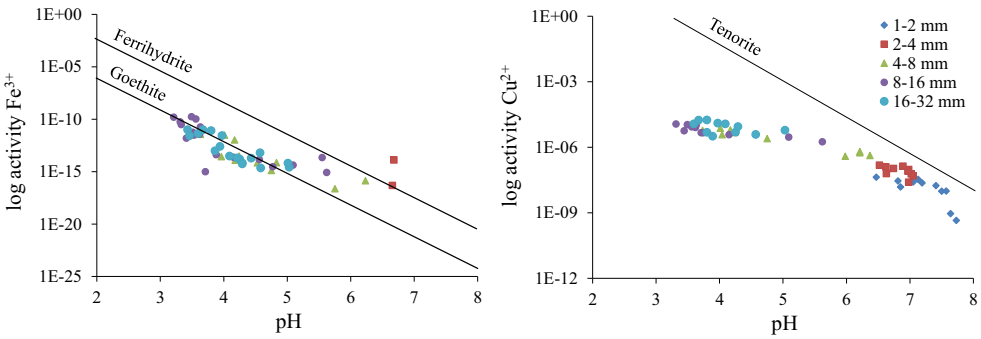

Fig. 7 Log of activities for Fe^{3+} with respect to ferrihydrite and goethite, and Cu^{2+} with respect to tenorite (*right*) plotted against pH

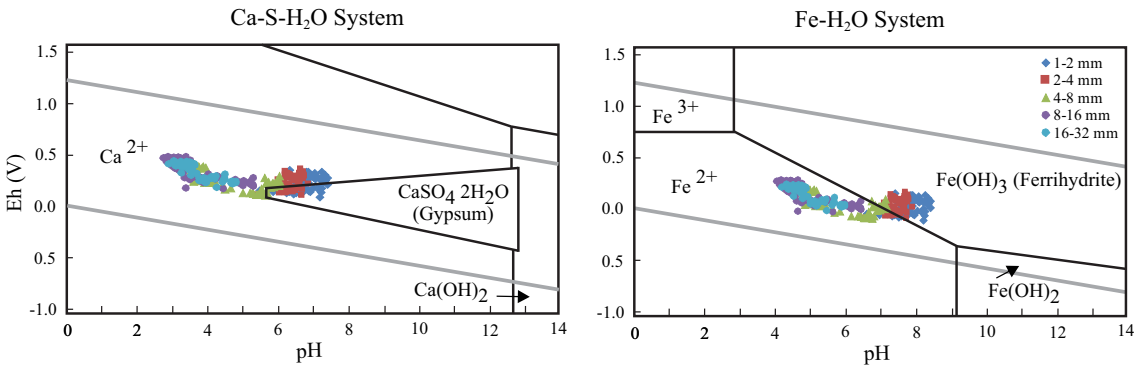

Fig. 8 Fe–H_2O and Ca–S–H_2O System modified from original HSC chemistry plot; input values in molality (mol/kg) at 20 °C. *Gray lines* indicate stability of water

effectiveness of rinsing plays a role in the resulting concentrations of the main ions Ca^{2+} and SO_4^2. In this case, the saturation of the leachates with Ca^{2+} and SO_4^{2-} for the finer grains reflects the high dissolution rate of the most likely source of these ions, calcite for Ca^{2+} and the oxidation of sulphides for SO_4^{2-}. Coarser grains did not plot gypsum formation, based on the Ca^{2+} and SO_4^{2-} concentration. This has two implications: first is that rinsing was effective in removing the Ca^{2+} and SO_4^{2-} that were produced during the acid generation and carbonate dissolution, and second is that the Eh–pH plot also depicts sulphide oxidation rates in the various grain sizes. As previously discussed, the finer grains have relatively higher Ca^{2+} and SO_4^{2-} production rates than the other grain sizes. This does not, however, suggest that gypsum formation is inhibited in the coarser grains since we do not know whether rinsing has indeed removed all the Ca^{2+} and SO_4^{2-} produced from the reactions.

Fe–H_2O System

The Fe stability diagram shows that ferrihydrite is more stable in the finer grains, while the coarser and intermediate grain sizes suggest Fe^{2+} stability. The weekly rinsing may not have dislodged most ferrihydrite in the finer grains, so they were supersaturated with respect to ferrihydrite. This suggests that most of the Fe^{3+} produced was removed as ferrihydrite.

Scaling and Field Implications

Kinetic tests are accelerated versions of what is anticipated to occur in a mine waste dump, so the issue of applying these results to an actual field setting can be difficult, due to factors that cannot be completely controlled in the laboratory. Strömberg and Banwart (1999b) suggested that mineralogy and slower weathering rates in the field due to variations in temperature and oxygen content can contribute to difficulties in scaling laboratory results to field scale. Pearce et al. (2015) noted that the use of laboratory leach column data for field estimates of intrinsic oxidation rate and seepage quality requires careful consideration, as scaling factors will considerably impact the validity of the results. In a study of sulphate release rates from Duluth Complex rock, Lapakko and Olson (2015) reported an empirically-based distribution of 714 scaling factors representing the ratio of field rates to laboratory rates showed that laboratory tests can be scaled to develop a probability distribution of predicted operational rates. Furthermore, they pointed out that the magnitude of scaling depends on the solute being scaled, drainage pH, rock type, composition, method of laboratory and field rate generation, and reaction rate variables (e.g. temperature, leachate to rock ratio, oxygen availability).

Please note that the results of this research only represent porphyry skarn Cu–Zn type rocks. The question of whether crushing to a maximum of 4 mm will result in neutral drainage pH is still subject to further studies; resulting leachate chemistry will vary for each type of material used. Water quality, such as pH of the mine water coming from the monitoring wells and flooded adits of the Recsk mine site, cannot be fully related to the results of this experiment. Although actual field water of some of the abandoned mine openings had pHs as low as 2.7 and a pe of 245 mV, spatial variation still must be considered, since current monitoring activities in the area may represent only the upper levels and may not actually reflect the effect or contribution of the porphyry skarn Cu–Zn rocks at the −900 m level. Care must be taken when applying these results to other conditions.

Conclusion

The effect of grain size on the quality of leachate produced from a kinetic test using a porphyry skarn Cu–Zn material with known mineralogy and textural characteristics was

studied for 85 weeks. Static testing suggests that all the grain size ranges started off with uniform total NP values, but that available NP value increased as grain size was reduced. Kinetic test results confirm that although reduction in grain size increased the available surface area for sulphide oxidation, it did not always produce an acidic pH. It was found that finer grains (1–2 and 2–4 mm) produced a circumneutral pH, while coarse grains (8–16 and 16–32 mm) produced an end pH of 3.0–4.0. An intermediate grain size, 4–8 mm, had a circumneutral pH for the first 40 weeks, and then pH dropped, ending at about 3.0 by the end of the test. This can be partly explained by the fact that available NP increased as the grain size decreased. The widely held general concept of a higher oxidation rate for finer grains due to an increased surface area was only applicable during the early periods of the experiment. In time, the surface area effects on the oxidation rate may be exceeded by other factors, such as oxygen availability, hydraulic factors, secondary mineral formation, and even bacterial activity.

Oxidation rate limiting factors are strongly correlated to variations in grain size. These were mainly identified as the availability of oxygen and water, which are vital for sulphide oxidation reactions. Bacterial activity and Fe^{3+} may have contributed significantly to the higher oxygen consumption rate for the coarser grains most especially for the 4–8 mm. Secondary minerals coating also limited and enhanced the oxidation-neutralization rates within the system, respectively. The effect of grain size on metal leaching cannot be fully established, but it is clearly pH-controlled. It was also observed that finer grains produced the highest concentration of Zn, while the coarser grains produced the highest concentrations of Fe.

Acknowledgments This research was made possible through funding and support from the Kjeøy Research and Education Center, Norway. This work was carried out in the Sustainable Resource Management Center of Excellence at the University of Miskolc as part of the TAMOP-4.2.2/A-11/1-KONV-2012-0049 "WELL aHEAD" project in the framework of the New Széchenyi Plan, funded by the European Union, co-financed by the European Social Fund. XRD, XRF, SEM–EDS, and all mineralogical characterization studies were performed at the University of Miskolc. We also acknowledge Dr. Ferenc Kristaly for conducting the XRD analysis and Ferenc Móricz for obtaining the data for the first 19 weeks of the experiment. We also extend our gratitude to Dr. Andrew Barnes of SRK-UK for his review and comments to help improve this manuscript.

References

Acero P, Cama P, Ayora C, Asta MP (2009) Chalcopyrite dissolution rate law from pH 1 to 3. Geol Acta 7(3):389–397

American Society of Testing Materials (ASTM) (2007) Standard test method for laboratory weathering of solid materials using humidity cell. American Soc for Testing and Materials. http://www.astm.org

Anderson M, Charer J, Nicholson R (1999) The oxygen consumption method (OCM): a new technique for quantifying sulphide oxidation rates in waste rock. In: Proceedings of the mining and the environment, pp 1133–1142

Bowell RJ, Sapsford DJ, Dey M, Williams KP (2006) Protocols affecting the reactivity of mine waste during laboratory-based kinetic tests. In: Proceedings of the 7th international conference on acid rock drainage (ICARD)

CEN/TC 292 (2009) Characterization of waste—static test for determination of acid potential and neutralisation potential of sulfidic waste. European Committee for Standardization

CEN/TR 16363 (2012) Characterization of waste—kinetic testing for assessing acid generation potential of sulphidic waste from extractive industries. European Committee for Standardization

Fergusson KD, Morin KA (1991) The prediction of acid rock drainage—lessons from the database. In: Proceedings of the 2nd international conference on the abatement of acidic drainage, vol 3, Montreal, QC, Canada, pp 85–106

Földessy J, Szebényi (2008) The mineralization of the Recsk Deeps and Lahoca—short geological overview. In: Proceedings of the University of Miskolc series A, mining, vol 73, pp 87–100. http://phd.lib.uni-miskolc.hu/JaDoX_Portlets/documents/document_13278_section_5414.pdf

Geidel G, Caruccio F, O'Hagan M (1983) An assessment of acid loads from various size fractions of sandstone and binder material. In: Proceedings of the symposium on surface mining, hydrology, sedimentology and reclamation, Lexington, KY, USA, pp 53–56

Hallberg KB (2010) New perspectives in acid mine drainage microbiology. Hydrometallurgy 104:448–453

Jambor JL, Blowes DW, Ritchie AIM (2003) Environmental aspects of mine wastes, vol 31. Mineralogical Association of Canada short course series, Vancouver

Lapakko K (1988) Prediction of acid mine drainage from Duluth Complex mining wastes in northeastern Minnesota. In: Proceedings of the mine drainage and surface mine reclamation conference, pp 180–190. http://www.asmr.us/Publications/Conference%20Proceedings/1988%20Vol%201/Lapakko%20180-190.pdf

Lapakko KA, Antonson DA (2006) Pyrite oxidation rates from humidity cell testing of greenstone rock. In: Proceedings of the 7th ICARD

Lapakko K, Olson M (2015) Scaling laboratory sulphate release rates to operational waste rock piles. In: Proceedings of the 10th ICARD

Lapakko K, Wessels J, Antonson D (1995) Long term dissolution testing of mine waste. US EPA Grant X-8200322-01-0, MN Department of Natural Resources. http://nepis.epa.gov/Adobe/PDF/2000EFQA.PDF

Lapakko K, Haub J, Antonson D (1998) Effects of dissolution time and particle size on kinetic test results. In: SME annual meeting and exhibition. http://wvmdtaskforce.com/proceedings/98/98LAP/98LAP.HTM

Lapakko KA, Engstrom JN, Antonson DA (2006) Effects of particle size on drainage quality from three lithologies. In: Proceedings of the 7th ICARD

Molnár F, Jung P, Kupi L, Pogány A, Vágó E, Viktorik O (2008) Epithermal zones of the porphyry–skarn–epithermal ore complexes at Recsk. In: Proceedings of the University of Miskolc series A, mining. http://www.matarka.hu/koz/ISSN_1219-008X/73k_2008_eng/ISSN_1219-008X_vol_73_2008_eng_099-128.pdf

Morin KA, Hutt NM (1994) An empirical technique for predicting the chemistry of water seeping from mine-rock piles. In: Proceedings of the international land reclamation and mine drainage conference and 3rd international conference on the abatement of acidic drainage, US Bureau of Mines SP 06A-94, pp 148–156

Morin KA, Hutt NM, Ferguson KD (1995). Measure rates of sulfide oxidation and acid neutralization in kinetic tests: statistical lessons from the database. In: Paper presented at Sudbury '95 conference on mining and the environment, pp 525–536. http://mdag.com/MDAG%20Paper%20Database/M0055%20-%20Morin%20et%20al%201995%20-%20Rates%20of%20Oxidation.PDF

Nordstrom DK (1982) Aqueous pyrite oxidation and the consequent formation of secondary iron minerals. In: Cedric KA, Fanning DS, Hossner IR (eds) Acid sulphate weathering. Soil Science of America special publication no. 10, pp 37–56

Parkhurst LB, Appelo CAJ (2012) User guide to PHREEQC (version 2). A computer program for speciation, batch reaction, one dimensional transport, and inverse geochemical calculation. USGS WRI Report 99-4259, Washington, DC

Parks GA (1990) Surface energy and adsorption at mineral–water interfaces: an introduction. Rev Mineral 23:133–175

Pearce S, Scott P, Weber P (2015) Waste rock dump geochemical evolution: matching lab data, models and predictions with reality. In: Proceedings of the 10th ICARD

Price WA (2009) Prediction manual for drainage chemistry from sulphidic geologic materials. MEND Report 1.20.1, Ottawa. http://www.abandoned-mines.org/pdfs/MENDPredictionManual-Jan05.pdf

Rimstidt DJ, Chermak JA, Gagen PM (1994) Chapter 1 rates of reaction of galena, sphalerite, chalcopyrite, and arsenopyrite with Fe(III) in acidic solutions. In: Alpers CN, Blowes DW (eds) Environmental geochemistry of sulfide oxidation. ACS symposium series. American Chemical Society, Washington, DC

Rosso KM, Becker U, Hochella M (1999) The interaction of pyrite 100 surfaces with O_2 and H_2O: fundamental oxidation mechanisms. Am Mineral 84:1549–1561

Rukezo G (2003) Drainage geochemistry of the Recsk-Lahoca mining area, Matra Mountains, Hungary. International Institute for Geo-Information Science and Earth Observation (ITC), Enschede

Schippers A, Breuker A, Blazejak A, Bosecker K, Kock D, Wright TL (2010) The biogeochemistry and microbiology of sulfidic mine waste and bioleaching dumps and heaps, and novel Fe(II)-oxidizing bacteria. Hydrometallurgy 104:342–350

Singer PC, Stumm W (1970) Acid mine drainage: the rate limiting step. Science 167:1121–1123

Smith L, LÓpez D, Beckie R, Morin K, Dawson R, Price W (1995) Hydrogeology of waste rock dumps. http://mend-nedem.org/wp-content/uploads/2013/01/1.Associate-Project-PA-1.pdf

Strömberg B, Banwart S (1999a) Experimental study of acidity-consuming processes in mining waste rock: some influences of mineralogy and particle size. Appl Geochem 14:1–16

Strömberg B, Banwart S (1999b) Weathering kinetics of waste rock from the Aitik copper mine, Sweden: scale dependent rate factors and pH controls in large column experiments. J Contam Hydrol 39:59–89

Walder I, Stormont J (2004) Thorough characterization of the hydrogeological and geochemical processes in waste rocks are essential for effective reclamation. In: Proceedings of the 6th international conference on clean technology for the mining industry